

1 Performances of site specific parameterizations of longwave  
2 radiation

3 Giuseppe Formetta<sup>1</sup>, Marialaura Bancheri<sup>2</sup>, Olaf David <sup>3</sup> and Riccardo Rigon <sup>2</sup>

4 <sup>1</sup>Centre for Ecology & Hydrology, Crowmarsh Gifford, Wallingford, UK

5 <sup>2</sup>Dipartimento di Ingegneria Civile Ambientale e Meccanica, Universita' degli Studi di Trento,  
6 Italy

7 <sup>3</sup>Dept. of Civil and Environmental Engineering, Colorado State University, Fort Collins, CO,  
8 USA

9 October 21, 2016

10 **Abstract**

11 In this work ten algorithms for estimating downwelling longwave atmospheric radiation ( $L_{\downarrow}$ ) and one for  
12 upwelling longwave radiation ( $L_{\uparrow}$ ) are integrated into the JGrass-NewAge modeling system. The algorithms  
13 are tested against energy flux measurements available for 24 sites in North America to assess their reliability.  
14 These new JGrass-NewAge model components are used i) to evaluate the performances of simplified models  
15 (SMs) of  $L_{\downarrow}$ , as presented in literature formulations, and ii) to determine by automatic calibration the  
16 site-specific parameter sets for  $L_{\downarrow}$  in SMs. For locations where calibration is not possible because of a lack of  
17 measured data, we perform a multiple regression using on-site variables, i.e. mean annual air temperature,  
18 relative humidity, precipitation, and altitude. The regressions are verified through a leave-one-out cross  
19 validation, which also gathers information about the possible errors of estimation. Most of the SMs, when  
20 executed with parameters derived from the multiple regressions, give enhanced performances compared to  
21 the corresponding literature formulation. A sensitivity analysis is carried out for each SM to understand  
22 how small variations of a given parameter influence SM performance. Regarding the  $L_{\downarrow}$  simulations, the  
23 Brunt (1932) and Idso (1981) SMs, in their literature formulations, provide the best performances in many  
24 of the sites. The site-specific parameter calibration improves SM performances compared to their literature  
25 formulations. Specifically, the root mean square error (RMSE) is almost halved and the Kling Gupta  
26 efficiency is improved at all sites. Also in this case Brunt (1932) and Idso (1981) SMs provided the best  
27 performances.

28 The  $L_{\uparrow}$  SM is tested by using three different temperatures (surface soil temperature, air temperature at  
29 2 m elevation, and soil temperature at 4 cm depth) and model performances are then assessed. Results show  
30 that the best performances are achieved using the surface soil temperature and the air temperature.

## 31 1 Introduction

32 Longwave radiation is an important component of the radiation balance on earth and it affects many phenom-  
33 ena, such as evapotranspiration, snow melt (Plüss and Ohmura, 1997), glacier evolution (MacDonell et al.,  
34 2013), vegetation dynamics (Rotenberg et al., 1998), plant respiration, and primary productivity (Leigh Jr,  
35 1999). Longwave radiation is usually measured with pyrgeometers, but these are not normally available in  
36 basic meteorological stations, even though an increasing number of projects has been developed to fill the gap  
37 Augustine et al. (2000), Augustine et al. (2005) and Baldocchi et al. (2001). The use of satellite products to  
38 estimate longwave solar radiation is increasing (GEWEX, Global Energy and Water cycle Experiment, ISCCP  
39 the International Satellite Cloud Climatology Project) but they have too coarse a spatial resolution for many  
40 hydrological uses. Therefore, models have been developed to solve energy transfer equations and compute ra-  
41 diation at the surface (e.g. Key and Schweiger (1998), Kneizys et al. (1988)). These physically based and fully  
42 distributed models provide accurate estimates of the radiation components. However, they require input data  
43 and model parameters that are not easily available. To overcome this issue, simplified models (SM), which are  
44 based on empirical or physical conceptualizations, have been developed to relate longwave radiation to atmo-  
45 spheric proxy data such as air temperature, water vapor deficit, and shortwave radiation. They are widely used  
46 and provide clear sky (e.g. Ångström (1915); Brunt (1932); Idso and Jackson (1969)) and all-sky estimations  
47 of downwelling ( $L_{\downarrow}$ ) and upwelling ( $L_{\uparrow}$ ) longwave radioation(e.g. Brutsaert (1975); Iziomon et al. (2003a)).

48 SM performances have been assessed in many studies by comparing measured and modeled  $L_{\downarrow}$  at hourly  
49 and daily time-steps (e.g. Sugita and Brutsaert (1993a); Iziomon et al. (2003b); Juszak and Pellicciotti (2013);  
50 MacDonell et al. (2013); Schmucki et al. (2014)). Hatfield et al. (1983) was among the first to present a  
51 comparison of the most used SMs in an evaluation of their accuracy. They tested seven clear-sky algorithms  
52 using atmospheric data from different stations in the United States. In order to validate the SMs under  
53 different climatic conditions, they performed linear regression analyses on the relationship between simulated  
54 and measured  $L_{\downarrow}$  for each algorithm. The results of the study show that the best models were Brunt (1932),  
55 Brutsaert (1975) and Idso (1981). Flerchinger et al. (2009) made a similar comparison using more formulations  
56 (13) and a wider data-set from North America and China, considering all possible sky conditions. Finally,  
57 Carmona et al. (2014) evaluated the performance of six SMs, with both literature and site-specific formulations,  
58 under clear-sky conditions for the sub-humid Pampean region of Argentina.

59 However, none of the above studies have developed a method to systematically estimate site-specific model  
60 parameters for location where measurements are not available using basic site characteristics.

61 This paper introduces the LongWave Radiation Balance package (LWRB) of the JGrass-NewAGE modelling  
62 system Formetta et al. (2014a). LWRB implements 10 formulations for  $L_{\downarrow}$  and one for  $L_{\uparrow}$  longwave radiation.  
63 The package was systematically tested against measured  $L_{\downarrow}$  and  $L_{\uparrow}$  longwave radiation data from 24 stations  
64 across the contiguous USA, chosen from the 65 stations of the AmeriFlux Network. Unlike all previous works,  
65 the LWRB component follows the specifications of the Object Modeling System (OMS) framework (David  
66 et al., 2013). Therefore, it can use all of the JGrass-NewAge tools for the automatic calibration algorithms,

67 data management and GIS visualization, and it can be seamlessly integrated into various modeling solutions  
 68 for the estimation of water budget fluxes (Formetta et al., 2014a). Moreover, differently from other studies, all  
 69 the tools used in this paper are open-source, well documented, and ready for practical use by other researchers  
 70 and practitioners.

## 71 2 Methodology

72 The SMs for  $L_{\uparrow}$  [ $\text{W m}^{-2}$ ] and  $L_{\downarrow}$  [ $\text{W m}^{-2}$ ] longwave radiation are based on the Stefan-Boltzmann equation:

$$73 \quad L_{\downarrow} = \epsilon_{all-sky} \cdot \sigma \cdot T_a^4 \quad (1)$$

$$76 \quad L_{\uparrow} = \epsilon_s \cdot \sigma \cdot T_s^4 \quad (2)$$

73 where  $\sigma = 5.670 \cdot 10^{-8}$  [ $\text{W m}^{-2} \text{ K}^{-4}$ ] is the Stefan-Boltzmann constant,  $T_a$  [K] is the air temperature,  $\epsilon_{all-sky}$   
 74 [-] is the effective atmospheric emissivity,  $\epsilon_s$  [-] is the soil emissivity and  $T_s$  [K] is the surface soil temperature.  
 75 To account for the increase of  $L_{\downarrow}$  in cloudy conditions,  $\epsilon_{all-sky}$  [-] is formulated according to eq. (3):

$$78 \quad \epsilon_{all-sky} = \epsilon_{clear} \cdot (1 + a \cdot c^b) \quad (3)$$

76 where  $c$  [-] is the cloud cover fraction and  $a$  [-] and  $b$  [-] are two calibration coefficients. Site specific values of  
 77  $a$  and  $b$  are presented in Brutsaert (1975), ( $a=0.22$  and  $b=1$ ), Iziomon et al. (2003a) ( $a$  ranges between 0.25 and  
 78 0.4 and  $b=2$ ) and Keding (1989) ( $a=0.183$  and  $b=2.18$ ). In our modeling system  $a$  and  $b$  are calibrated to fit  
 79 measurement data under all-sky conditions. The cloud cover fraction,  $c$ , can be estimated from solar radiation  
 80 measurements (Crawford and Duchon, 1999), from visual observations (Alados-Arboledas et al., 1995, Niemelä  
 81 et al., 2001), and from satellite data (Sugita and Brutsaert, 1993b) or it can be modeled as well. In this study  
 82 we use the formulation presented in Campbell (1985) and Flerchinger (2000), where  $c$  is related to the clearness  
 83 index  $s$  [-], i.e. the ratio between the measured incoming solar radiation,  $I_m$  [ $\text{W m}^{-2}$ ], and the theoretical solar  
 84 radiation computed at the top of the atmosphere,  $I_{top}$  [ $\text{W m}^{-2}$ ], according to  $c = 1 - s$  (Crawford and Duchon,  
 85 1999). This type of formulation needs a shortwave radiation balance model to estimate  $I_{top}$  and meteorological  
 86 stations to measure  $I_m$ ; also, it cannot estimate  $c$  at night. In our application, the fact that the SMs are fully  
 87 integrated into the JGrass-NewAge system allows us to use the shortwave radiation balance model (Formetta  
 88 et al., 2013) to compute  $I_{top}$ . Night-time values of  $c$  are computed with a linear interpolation between its values  
 89 at the last hour of daylight and the first hour of daylight on consecutive days. The computation of the first  
 90 and last hour of the day is based on the model proposed in Formetta et al., 2013 that follows the approach  
 91 proposed in Corripio (2002), equations (4.23)-(4.25). The sunrise occurs at  $t = 12 \cdot (1 - \omega/\pi)$  and the sunset  
 92 will be at  $t = 12 \cdot (1 + \omega/\pi)$  where  $\omega$  is the hour angle, i.e. the angle between the observer meridian and the  
 93 solar meridian. It is zero at noon and positive before noon. Those equations are based on the assumption that

94 sunrise and sunset occur at the time when the z coordinate of the sun vector equals zero.

95 The formulation presented in equation (3) was proposed by Bolz (1949) applied in other studies (Carmona  
96 et al. (2014), Maykut and Church (1973), Jacobs (1978), Niemelä et al. (2001)). Evaluating the effectiveness of  
97 different formulations respect to equation (3) is still an open question which is not object of the current paper.  
98 It has been investigated in several studies (i.e. Flerchinger et al. (2009), Juszak and Pellicciotti (2013), and  
99 references therein) and some of them recommended the one proposed by Unsworth and Monteith (1975).

100 Ten SMs from literature have been implemented for the computation of  $\epsilon_{clear}$ . Table 1 specifies assigned  
101 component number, component name, defining equation, and reference to the paper from which it is derived.  
102 X, Y and Z are the parameters provided in literature for each model, listed in Table 2.

ID	Name	Formulation	Reference
1	Angstrom	$\epsilon_{clear} = X - Y \cdot 10^{Ze}$	Angström (1915)
2	Brunt's	$\epsilon_{clear} = X + Y \cdot e^{0.5}$	Brunt (1932)
3	Swinbank	$\epsilon_{clear} = (X \cdot 10^{-13} \cdot T_a^6) / (\sigma \cdot T_a^4)$	Swinbank (1963)
4	Idso and Jackson	$\epsilon_{clear} = 1 - X \cdot \exp(-Y \cdot 10^{-4} \cdot (273 - T_a)^2)$	Idso and Jackson (1969)
5	Brutsaert	$\epsilon_{clear} = X \cdot (e/T_a)^{1/Z}$	Brutsaert (1975)
6	Idso	$\epsilon_{clear} = X + Y \cdot 10^{-4} \cdot e \cdot \exp(1500/T_a)$	Idso (1981)
7	Monteith and Unsworth	$\epsilon_{clear} = X + Y \cdot \sigma \cdot T_a^4$	Monteith and Unsworth (1990)
8	Konzelmann	$\epsilon_{clear} = X + Y \cdot (e/T_a)^{1/8}$	Konzelmann et al. (1994)
9	Prata	$\epsilon_{clear} = [1 - (X + w) \cdot \exp(-(Y + Z \cdot w)^{1/2})]$	Prata (1996)
10	Dilley and O'Brien	$\epsilon_{clear} = (X + Y \cdot (T_a/273.16)^6 + Z \cdot (w/25)^{1/2}) / (\sigma \cdot T_a^4)$	Dilley and O'Brien (1998)

**Table 1:** Clear sky emissivity formulations:  $T_a$  is the air temperature [K],  $w$  [kg/m<sup>2</sup>] is precipitable water = 4650 [e<sub>0</sub>/T<sub>a</sub>] and  $e$  [kPa] is screen-level water-vapour pressure. The models follow the formulations presented in used in Flerchinger (2000). The Angstrom and Brunt model was presented as cited by Niemelä et al. (2001). Konzelmann uses water vapour pressure in [Pa] not [kPa].

103 The models presented in Table 1 were proposed with coefficient values (X, Y, Z) strictly related to the location  
104 in which the authors applied the model and where measurements of  $L_{\downarrow}$  radiation were collected. Coefficients  
reflect climatic, atmospheric and hydrological conditions of the sites, and are reported in Table 2.

ID	Name	X	Y	Z
1	Angstrom	0.83	0.18	-0.07
2	Brunt	0.52	0.21	[—]
3	Swinbank	5.31	[—]	[—]
4	Idso and Jackson	0.26	-7.77	[—]
5	Brutsaert	1.72	7	[—]
6	Idso	0.70	5.95	[—]
7	Monteith and Unsworth	-119.00	1.06	[—]
8	Konzelmann et al	0.23	0.48	[—]
9	Prata	1.00	1.20	3.00
10	Dilley and O'brien	59.38	113.70	96.96

**Table 2:** Model parameter values as presented in their literature formulation.

105  
106 The formulation of the  $L_{\uparrow}$  requires the soil emissivity, which usually is a property of the nature of a surface,  
107 and the surface soil temperature. Table 3 shows the literature values (Brutsaert, 2005) of the soil emissivity for  
108 different surface types:  $\epsilon_s$  varies from a minimum of 0.95 for bare soils to a maximum of 0.99 for fresh snow.

109 It is well known that surface soil temperature measurements are only available at a few measurement sites,  
110 therefore, under the hypothesis that difference between soil and air temperatures is not too big, it is possible to  
111 simulate  $L_{\uparrow}$  using the air temperature (Park et al., 2008). In our approach three different types of temperature

Nature of surface	Emissivity
Bare soil (mineral)	0.95 – 0.97
Bare soil (organic)	0.97 – 0.98
Grassy vegetation	0.97 – 0.98
Tree vegetation	0.96 – 0.97
Snow (old)	0.97
Snow (fresh)	0.99

**Table 3:** Soil emissivity for surface types (Brutsaert, 2005).

were used to simulate  $L_{\uparrow}$ , specifically: surface soil temperature (where available), air temperature at 2 m height, and soil temperature at 4 cm depth.

The LWRB package (see flowchart in Figure1) is part of the JGrass-NewAge system and was preliminary tested in Formetta et al. (2014b). Model inputs depend on the specific SM being implemented and the purpose of the run being performed (calibration, verification, simulation). The inputs are meteorological observations such as air temperature, relative humidity, incoming solar radiation, and sky clearness index. The LWRB is also fed by other JGrass-NewAGE components, such as the shortwave radiation balance (SWRB) (Formetta et al., 2013). To test model performances (i.e. verification), the LWRB can be connected to the system's Verification component; to execute the parameter calibration algorithm (Formetta et al., 2014a), it can be connected to the LUCA (Let Us CALibrate) component. In turn, all these components can and/or need to be connected to other ones, as the problem under examination may require. Model outputs are  $L_{\downarrow}$  and  $L_{\uparrow}$ . These can be provided in single points of specified coordinates or over a whole geographic area, represented as a raster map. For the latter case a digital elevation model (DEM) of the study area is necessary in input.

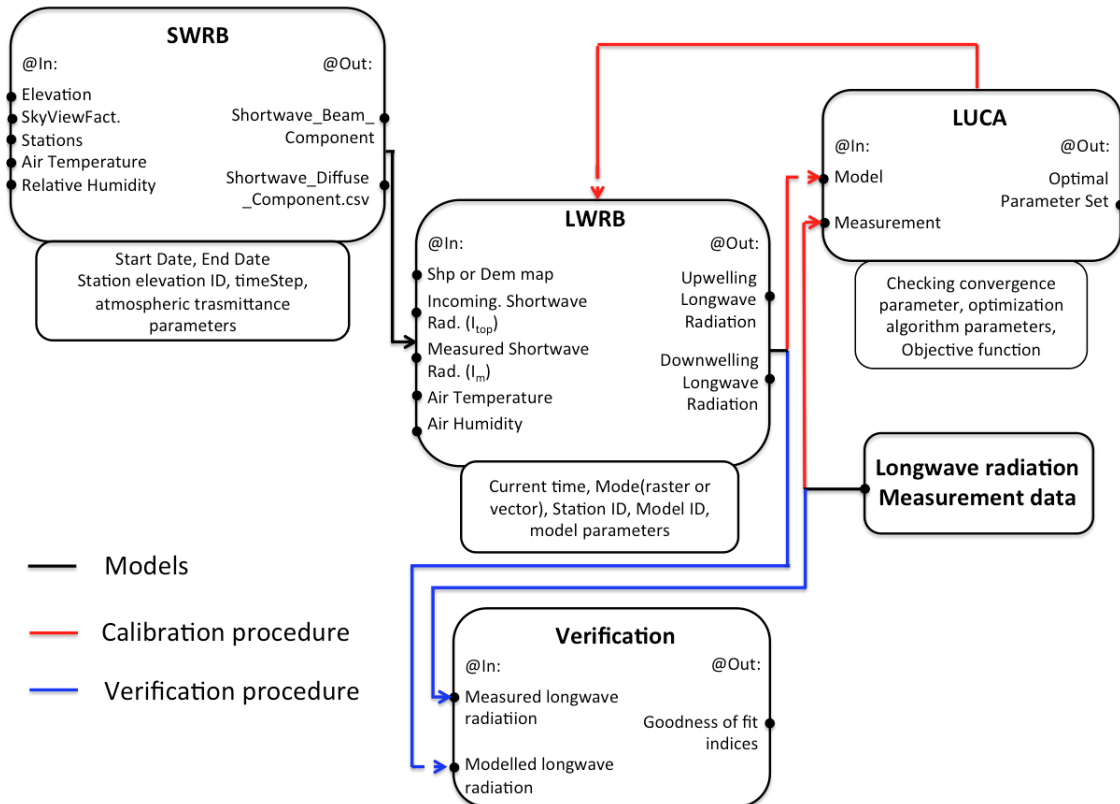


**Figure 1:** The LWRB component of JGrass-NewAge and the flowchart to model longwave radiation.

125 The subsection 2.1 and 2.2 respectively present the calibration and the verification procedure. Moreover  
126 a model sensitivity analysis procedure is presented in subsection 2.3 and a multi-regression model to relate  
127 optimal parameter set and easy available meteorological data is proposed in subsection 2.4.

128 **2.1 Calibration of  $L_{\downarrow}$  longwave radiation models**

129 Model calibration estimates the site-specific parameters of  $L_{\downarrow}$  models by tweaking them with a specific algorithm  
130 in order to best fit measured data. To this end, we use the LUCA calibration algorithm proposed in Hay et al.  
131 (2006), which is a part of the OMS core and is able to optimize parameters of any OMS component. LUCA  
132 is a multiple-objective, stepwise, and automated procedure. As with any automatic calibration algorithm, it is  
133 based on two elements: a global search algorithm; and the objective function(s) to evaluate model performance.  
134 In this case, the global search algorithm is the Shuffled Complex Evolution, which has been widely used and  
135 described in literature (e.g., Duan et al., 1993). As the objective function we use the Kling-Gupta Efficiency  
136 (KGE, Gupta et al. (2009)), which is described below, but LUCA could use other objective functions just as  
137 well.

138 The calibration procedure for  $L_{\downarrow}$  follows these steps:

- 139 • The theoretical solar radiation at the top of the atmosphere ( $I_{top}$ ) is computed using the SWRB (see  
140 Figure 1);
- 141 • The clearness index,  $c$ , is calculated as the ratio between the measured incoming solar radiation ( $I_m$ ) and  
142  $I_{top}$ ;
- 143 • Clear-sky and cloud-cover hours are detected by a threshold on the clearness index (equal to 0.6), providing  
144 two subsets of measured  $L_{\downarrow}$ , which are  $L_{\downarrow clear}$  and  $L_{\downarrow cloud}$ . On one side, a threshold of 0.6 to define the  
145 clear-sky conditions helps in the sense that allow to define time-series of measured clear-sky  $L_{\downarrow}$  with  
146 comparable length in all the stations, and this is useful for a reliable calibration process. On the other  
147 side, it introduces a small error in computing the emissivity in all-sky condition using equation (3).  
148 Although the effects of this small error would need further investigations, they could be compensated  
149 by the optimization of the parameters  $a$  and  $b$ , that are non-linearly related to the emissivity in all-sky  
150 conditions;
- 151 • The parameters X, Y, and Z for the models in Table 1 are optimised using the subset  $L_{\downarrow clear}$  and setting  
152  $a=0$  in eq. 3;
- 153 • The parameters  $a$  and  $b$  for eq. 3 are optimized using the subset  $L_{\downarrow cloud}$  and using the X, Y, and Z values  
154 computed in the previous step.

155 The calibration procedure provides the optimal set of parameters at a given location for each of the ten  
156 models.

157 As well as parameter calibration, we carry out a model parameter sensitivity analysis and we provide a  
 158 linear regression model relating a set of site-specific optimal parameters with mean air temperature, relative  
 159 humidity, precipitation, and altitude.

## 160 2.2 Verification of $L_{\downarrow}$ and $L_{\uparrow}$ longwave radiation models

161 As presented in previous applications (e.g. Hatfield et al. (1983), Flerchinger et al. (2009)), we use the SMs  
 162 with the original coefficients from literature (i.e. the parameters of Table 2) and compare the performances of  
 163 the models against available measurements of  $L_{\downarrow}$  and  $L_{\uparrow}$  for each site. The goodness of fit is evaluated by using  
 164 two goodness-of-fit estimators: the Kling-Gupta Efficiency (KGE) and the root mean square error (RMSE).

165 The KGE (eq. 4) is able to incorporate into one objective function three different statistical measures of  
 166 the relation between measured (M) and simulated (S) data: (i) the correlation coefficient,  $r$  ; (ii) the variability  
 167 error,  $a = \sigma_S/\sigma_M$ ; and (iii) the bias error,  $b = \mu_S/\mu_M$ . In these definitions  $\mu_S$  and  $\mu_M$  are the mean values,  
 168 while  $\sigma_S$  and  $\sigma_M$  are the standard deviations, of measured and simulated time series.

$$169 KGE = 1 - \sqrt{(r - 1)^2 + (a - 1)^2 + (b - 1)^2} \quad (4)$$

169 The RMSE, on the other hand, is presented in eq. 5:

$$170 RMSE = \sqrt{\frac{1}{N} \sum_{i=1}^N (M_i - S_i)^2} \quad (5)$$

170 where M and S represents the measured and simulated time-series respectively and N is their length.

## 171 2.3 Sensitivity analysis of $L_{\downarrow}$ models

172 For each  $L_{\downarrow}$  model we carry out a model parameters sensitivity analysis to investigate the effects and significance  
 173 of parameters on performance for different model structures (i.e. models with one, two, and three parameters).  
 174 The analyses are structured according to the following steps:

- 175 • we start with the optimal parameter set, computed by the optimization process for the selected model;
- 176 • all parameters are kept constant and equal to the optimal parameter set, except for the parameter under  
 177 analysis;
- 178 • 1000 random values of the analyzed parameter are picked from a uniform distribution centered on the  
 179 optimal value with width equal to  $\pm 30\%$  of the optimal value; in this way 1000 model parameter sets  
 180 were defined and 1000 model runs were performed;
- 181 • 1000 values of KGE are computed by comparing the model outputs with measured time series.

182 The procedure was repeated for each parameter of each model and for each station of the analyzed dataset.

183 **2.4 Regression model for parameters of  $L_{\downarrow}$  models**

184 The calibration procedure previously presented to estimate the site specific parameters for  $L_{\downarrow}$  models requires  
185 measured downwelling longwave data. Because these measurements are rarely available, we implement a  
186 straightforward multivariate linear regression (Chambers et al., 1992; Wilkinson and Rogers, 1973) to relate  
187 the site-specific parameters X, Y and Z to a set of easily available site specific climatic variables, used as regres-  
188 sors  $r_i$ . To perform the regression we use the open-source R software (<https://cran.r-project.org>) and to select  
189 the best regressors we use algorithms known as "best subsets regression", which are available in all common  
190 statistical software packages. The regressors we have selected are: mean annual air temperature, relative hu-  
191 midity, precipitation, and altitude. The models that we use for the three parameters are presented in equations  
192 (6), (7), and (8):

$$X = i_X + \sum_{k=1}^N \alpha_k \cdot r_k + \epsilon_X \quad (6)$$

$$Y = i_Y + \sum_{k=1}^N \beta_k \cdot r_k + \epsilon_Y \quad (7)$$

$$Z = i_Z + \sum_{k=1}^N \gamma_k \cdot r_k + \epsilon_Z \quad (8)$$

193 where N=4 is the number of regressors (annual mean air temperature, relative humidity, precipitation, and  
194 altitude);  $r_k$  with  $k=1, \dots, 4$  are the regressors;  $i_X$ ,  $i_Y$ , and  $i_Z$  are the intercepts;  $\alpha_k$ ,  $\beta_k$ , and  $\gamma_k$  are the coefficients;  
195 and  $\epsilon_X$ ,  $\epsilon_Y$ , and  $\epsilon_Z$  are the normally distributed errors. Once the regression parameters are determined, the  
196 end-user can estimate site specific X, Y and Z parameter values for any location by simply substituting the  
197 values of the regressors in the model formulations.

198 **3 The study area: the AmeriFlux Network**

199 To test and calibrate the LWRB SMs we use 24 meteorological stations of the AmeriFlux Network (<http://ameriflux.ornl.gov>).  
200 AmeriFlux is a network of sites that measure water, energy, and CO<sub>2</sub> ecosystem fluxes in North and South  
201 America. The dataset is well-known and used in several applications such as Xiao et al. (2010), Barr et al.  
202 (2012), and Kelliher et al. (2004). Data used in this study are the Level 2, 30-minute average data. Complete  
203 descriptions and downloads are available at the Web interface located at <http://public.ornl.gov/ameriflux/>.

204 We have chosen 24 sites that are representative of most of the contiguous USA and span a wide climatic range:  
205 going from the arid climate of Arizona, where the average air temperature is 16 °C and the annual precipitation  
206 is 350 mm, to the equatorial climate of Florida, where the average air temperature is 24 °C and the annual  
207 precipitation is 950 mm. Some general and climatic characteristics for each site are summarized in Table 4, while  
208 Figure 2 shows their locations. The 30-minute average data have been cumulated to obtain continuous time  
209 series of averaged, hourly data for longwave radiation, air and soil temperature, relative humidity, precipitation,

210 and soil water content. Longwave radiation was measured with Eppley Pyrgeometers with uncertainty of +/-  
 211 3 [W m<sup>-2</sup>].

SiteID	State	Latitude	Longitude	Elevation (m)	Climate	T (°C)	Data period
1	AZ	31.908	-110.840	991	semiarid	19	2008 – 2013
2	AZ	31.591	-110.509	1469	temperate,arid	16	2002 – 2011
3	AZ	31.744	-110.052	1372	temperate,semi-arid	17	2007 – 2013
4	AZ	31.737	-109.942	1531	temperate,semi-arid	17	2004 – 2013
5	AZ	31.821	-110.866	116	subtropical	19	2004 – 2014
6	AZ	35.445	-111.772	2270	warm temperate	9	2005 – 2010
7	AZ	35.143	-111.727	2160	warm temperate	9	2005 – 2010
8	AZ	35.089	-111.762	2180	warm temperate	8	2005 – 2010
9	CA	37.677	-121.530	323	mild	16	2010 – 2012
10	CA	38.407	-120.951	129	mediterranean	15	2000 – 2012
11	FL	25.365	-81.078	0	equatorial savannah	24	2004 – 2011
12	ME	45.207	-68.725	61	temperate continental	5	1996 – 2008
13	ME	45.204	-68.740	60	temperate continental	6	1996 – 2009
14	MN	44.995	-93.186	301	continental	6	2005 – 2009
15	MN	44.714	-93.090	260	snowy, humid summer	8	2003 – 2012
16	MO	38.744	-92.200	219	temperate continental	13	2004 – 2013
17	MT	48.308	-105.102	634	continental	5	2000 – 2008
18	NJ	39.914	-74.596	30	temperate	12	2005 – 2012
19	OK	36.427	-99.420	611	cool temperate	15	2009 – 2012
20	TN	35.931	-84.332	286	temperate continental	15	2005 – 2011
21	TN	35.959	-84.287	343	temperate	14	1994 – 2007
22	TX	29.940	-97.990	232	warm temperate	20	2004 – 2012
23	WA	45.821	-121.952	371	strongly seasonal	9	1998 – 2013
24	WV	39.063	-79.421	994	temperate	7	2004 – 2010

**Table 4:** Some general and climatic characteristics of the sites used for calibration: elevation is the site elevation above sea level, T is the annual average temperature, and data period refers to the period of available measurements.

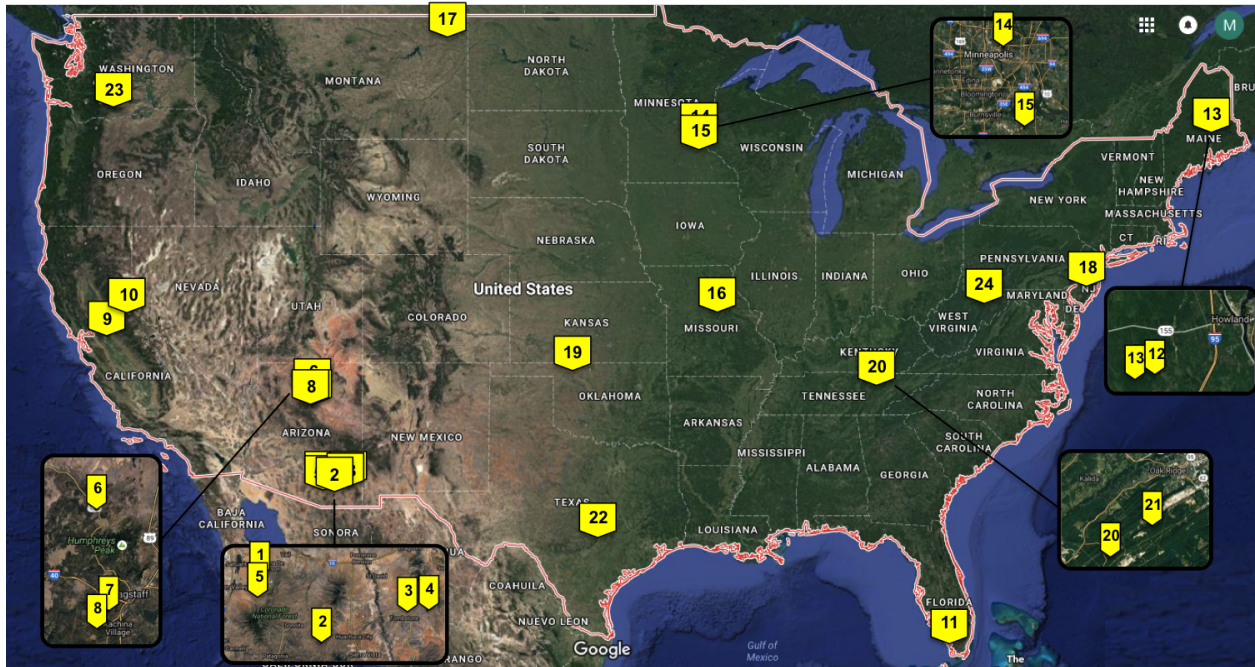


**Figure 2:** Test site locations in the United States of America.

212 **4 Results**

213 **4.1 Verification of  $L_{\downarrow}$  models with literature parameters**

214 When implementing the ten  $L_{\downarrow}$  SMs using the literature parameters, in many cases, they show a strong bias in  
215 reproducing measured data. A selection of representative cases is presented in Figure 3 which shows scatterplots  
216 for four SMs in relation to one measurement station. The black points represent the hourly estimates of  $L_{\downarrow}$   
217 provided by literature formulations, while the solid red line represents the line of optimal predictions. Model 1  
218 (Ångström (1915)) shows a tendency to lie below the 1:1 line, indicating a negative bias (percent bias of -9.8)  
219 and, therefore, an underestimation of  $L_{\downarrow}$ . In contrast, model 9 ( Prata (1996)) shows an overestimation of  $L_{\downarrow}$   
220 with a percent bias value of 26.3.

221 Figure 4 presents the boxplot of KGE (first column) and RMSE (second column) obtained for each model  
222 under clear-sky conditions, grouped by classes of latitude and longitude. In general all the models except the  
223 Model 8 (Konzelmann et al. (1994)) provided values of KGE higher than 0.5 and RMSE lower than 100 [W  
224  $m^{-2}$ ] for all the latitude and longitude classes. Model 8 is the less performing model for many of the stations  
225 likely because the model parameters were estimated for the Greenland where snow and ice play a fundamental  
226 role on the energy balance. Its KGE values range between 0.33 and 0.62 on average, while its RMSE values  
227 are higher than 100 [W  $m^{-2}$ ] except for latitude classes  $>40^{\circ}\text{N}$  and longitude classes  $>-70^{\circ}\text{W}$ . Model 6 (Idso  
228 (1981)) and Model 2 (Brunt (1932)) provide the best results and the lower variability, independently of the  
229 latitude and longitude ranges where they are applied. Their average KGE values are between 0.75 and 0.92,  
230 while the RMSE has a maximum value of 39 [W  $m^{-2}$ ]. Moreover, all the models except 2 and 6 show a high  
231 variability of the goodness of fit through the latitude and longitude classes.

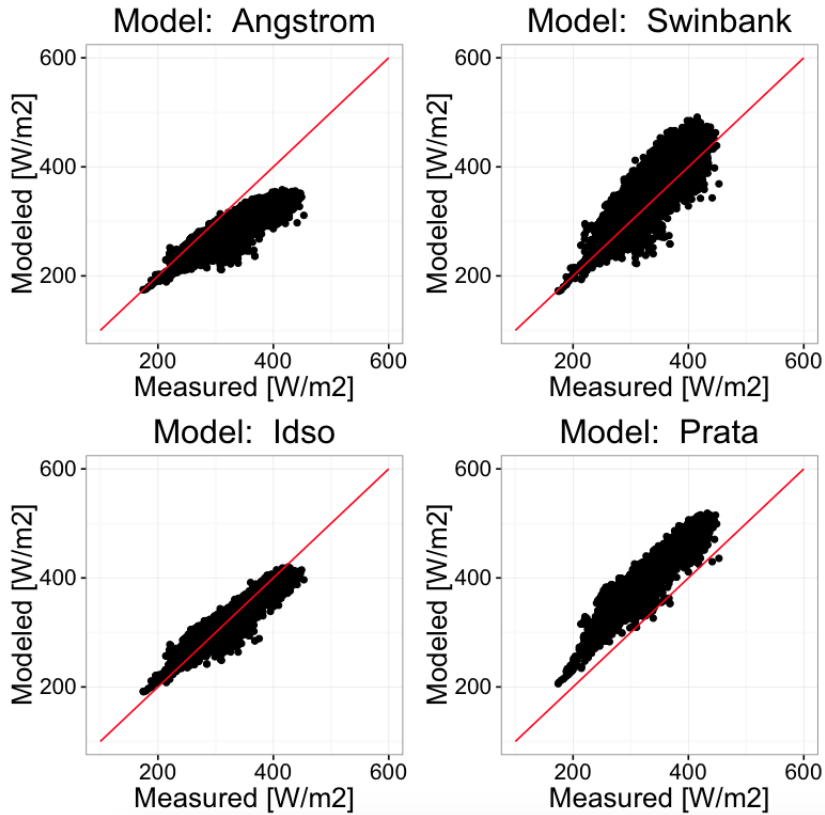


**Figure 3:** Results of the clear-sky simulation for four literature models using data from Howland Forest (Maine).

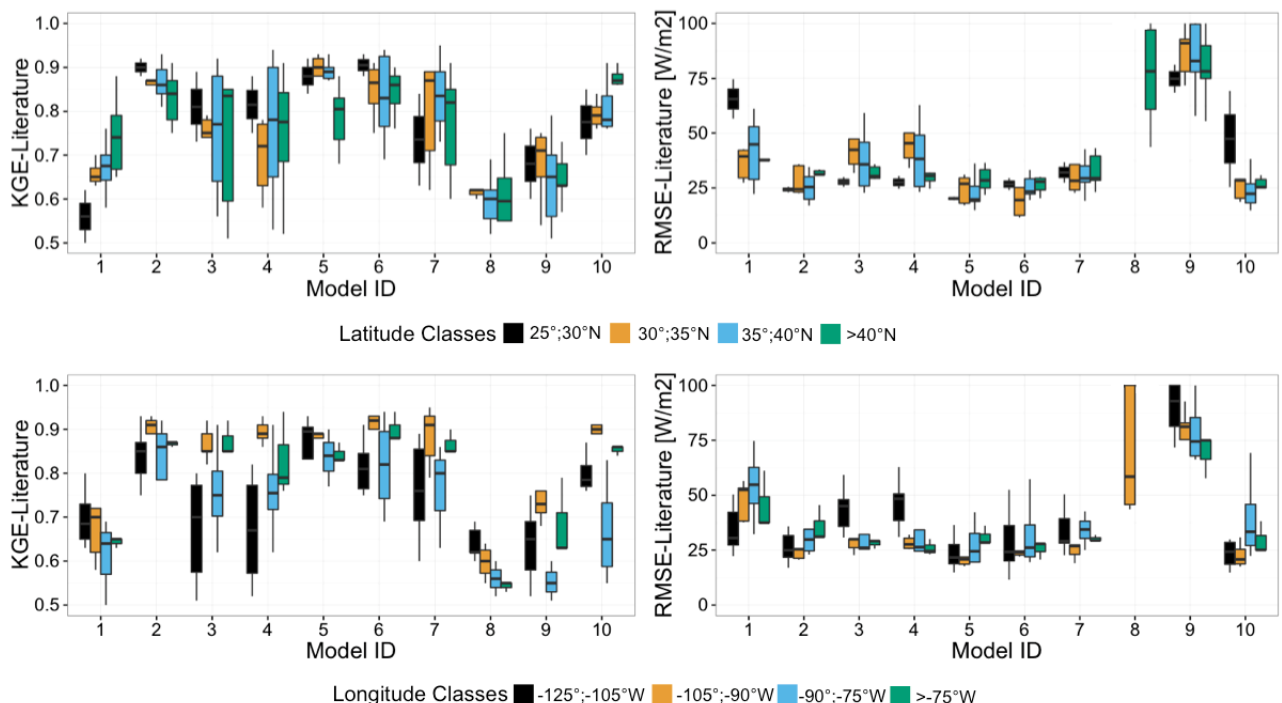


**Figure 4:** KGE and RMSE values for each clear-sky simulation using literature formulations, grouped by classes of latitude and longitude. Only values of KGE above 0.5 are shown. Only values of RMSE below 100 [W m<sup>-2</sup>] are shown.

## 232 4.2 $L_{\downarrow}$ models with site-specific parameters

233 The calibration procedure greatly improves the performances of all ten SMs. Optimized model parameters for  
 234 each model are reported in the supplementary material (Table S1). Figure 5 presents the boxplots of KGE and  
 235 RMSE values for clear-sky conditions grouped by classes of latitude and longitude. The percentage of KGE  
 236 improvement ranges from its maximum value of 70% for Model 8 (which is not, however, representative of the  
 237 mean behavior of the SMs) to less than 10% for Model 6, with an average improvement of around 35%. Even  
 238 though variations in model performances with longitude and latitude classes still exist when using optimized  
 239 model parameters, the magnitude of these variations is reduced with respect to the use of literature formulations.  
 240 The calibration procedure reduces the RMSE values for all the models to below 45 [W m<sup>-2</sup>], even for Model  
 241 8, which also in this case had the maximum improvement. Model 6 (Idso (1981)) and Model 2 (Brunt (1932))  
 242 provide the best results on average for all the analyzed latitude and longitude classes.

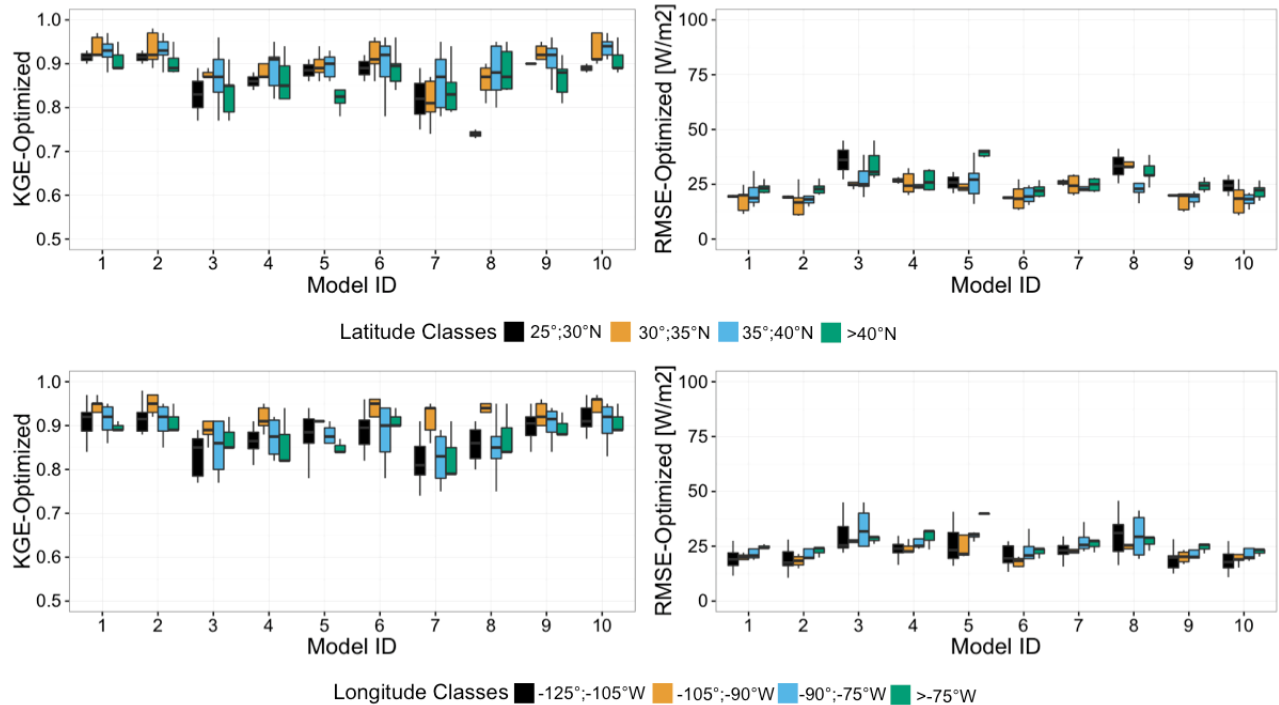


**Figure 5:** KGE (best is 1) and RMSE (best is 0) values for each optimized formulation in clear-sky conditions, grouped by classes of latitude and longitude. Only values of KGE above 0.5 are shown.

243 Figure 6 presents the boxplots of KGE and RMSE values for each model under all-sky conditions, grouped  
 244 by latitude and longitude classes. In general, for all-sky conditions we observe a deterioration of KGE and  
 245 RMSE values with respect to the clear-sky optimized case, with a decrease in KGE values up to a maximum of  
 246 25% on average for Model 10. This may be due to uncertainty incorporated in the formulation of the cloudy-sky  
 247 correction model (eq. 3): it seems that sometimes the cloud effects are not accounted for appropriately. This,  
 248 however, is in line with the findings of Carmona et al. (2014).

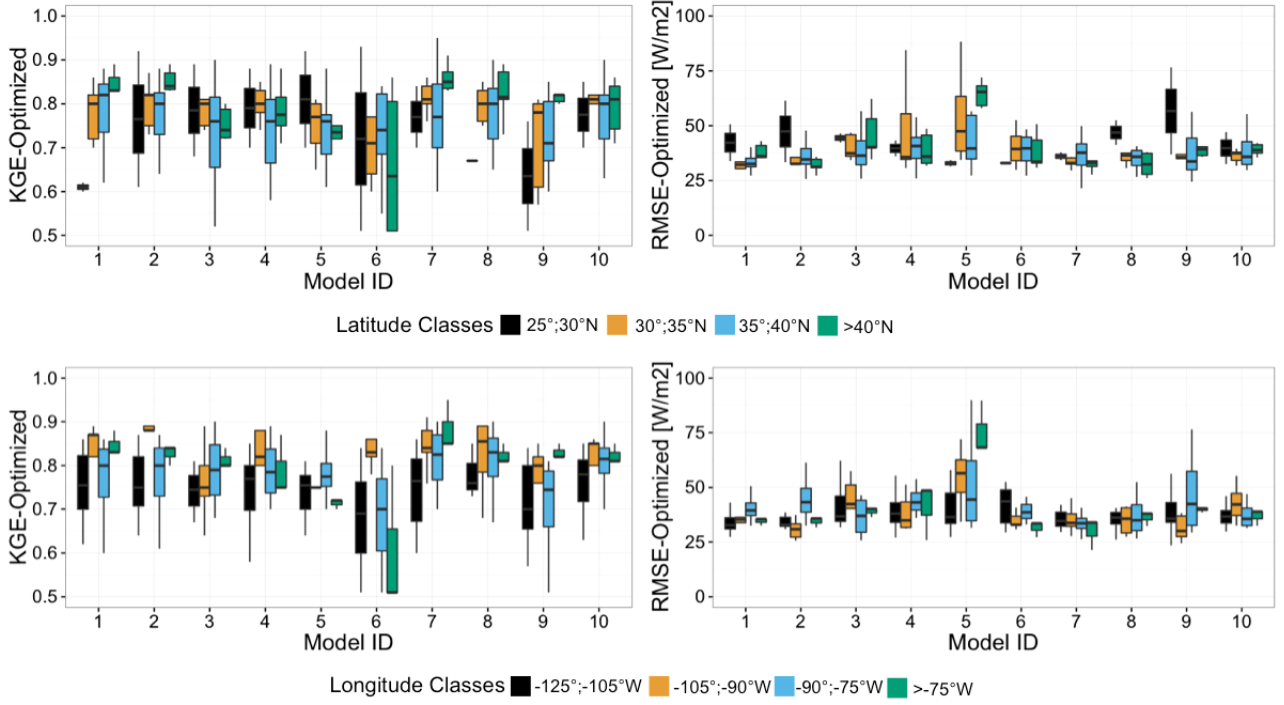


**Figure 6:** KGE and RMSE values for each model in all-sky conditions with the optimized parameters; results are grouped by classes of latitude and longitude. Only values of KGE above 0.5 are shown.

### 249 4.3 Sensitivity analysis of $L_{\downarrow}$ models

250 The results of the models sensitivity analysis are summarized in Figures 7-a and 7-b for models 1 to 5 and  
 251 models 6 to 10, respectively. Each figure presents three columns, one for each parameter. Considering model 1  
 252 and parameter X: the range of X is subdivided into ten equal-sized classes and for each class the corresponding  
 253 KGE values are presented as a boxplot. A smooth blue line passing through the boxplot medians is added to  
 254 highlight any possible pattern to parameter sensitivity. A flat line indicates that the model is not sensitive to  
 255 parameter variation around optimal value. Results suggest that models with one and two parameters are all  
 256 sensitive to parameter variation, presenting a peak in KGE in correspondence with their optimal values; this is  
 257 more evident in models with two parameters. Models with three parameters tend to have at least one insensitive  
 258 parameter, except for Model 1, that could reveal a possible overparameterization of the modeling process.

### 259 4.4 Regression model for parameters of $L_{\downarrow}$ models

260 A multivariate linear regression model was estimated to relate the site-specific parameters X, Y and Z to mean  
 261 annual air temperature, relative humidity, precipitation, and altitude. The script containing the regression  
 262 model is available, as specified in Reproducible Research section below.

263 The performances of the  $L_{\downarrow}$  models using parameters assessed by linear regression are evaluated through  
 264 the leave-one-out cross validation (Efron and Efron, 1982). We use 23 stations as training-sets for equations  
 265 (6), (7), and (8) and we perform the model verification on the remaining station. The procedure is repeated for  
 266 each of the 24 stations.

267 The cross validation results for all  $L_{\downarrow}$  models and for all stations are presented in Figures (8) and (9),

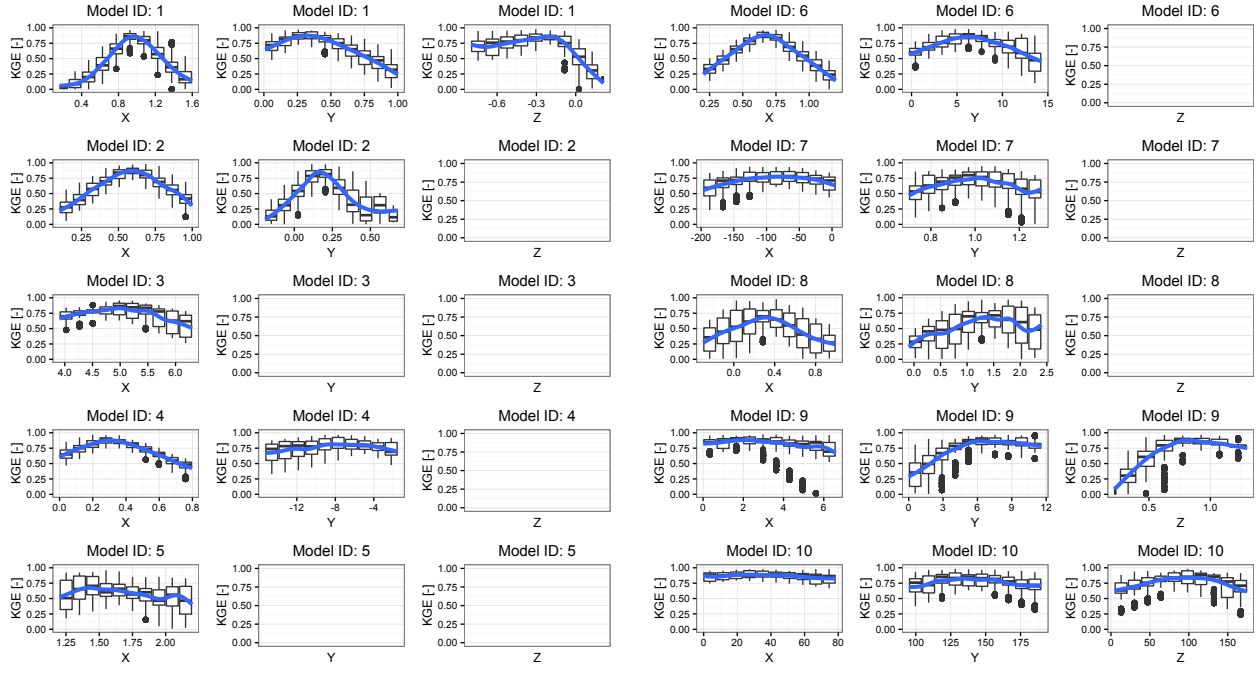


**Figure 7:** Results of the model parameters sensitivity analysis. It presents as boxplot the variation of the model performances due to a variation of one of the optimal parameter and assuming constant the others. The procedure is repeated for each model and the blue line represents the smooth line passing through the boxplot medians.

grouped by classes of latitude and longitude, respectively. They report the KGE comparison between the  $L_{\downarrow}$  models with their original parameters (in black) and with the regression model parameters (in black).

In general, the use of parameters estimated with regression model gives a good estimation of  $L_{\downarrow}$ , with KGE values of up to 0.92. With respect to the classic formulation, model performance with regression parameters improved for all the models independently of the latitude and longitude classes. In particular for Model 8 the KGE improved from 0.26 for the classic formulation to 0.92, on average. Finally, the use of the parameters estimated by the regression model provides a reduction of the model performances variability for all the models except Model 5 and 8, for longitude class -125;-105°W and -105;-90°W respectively.

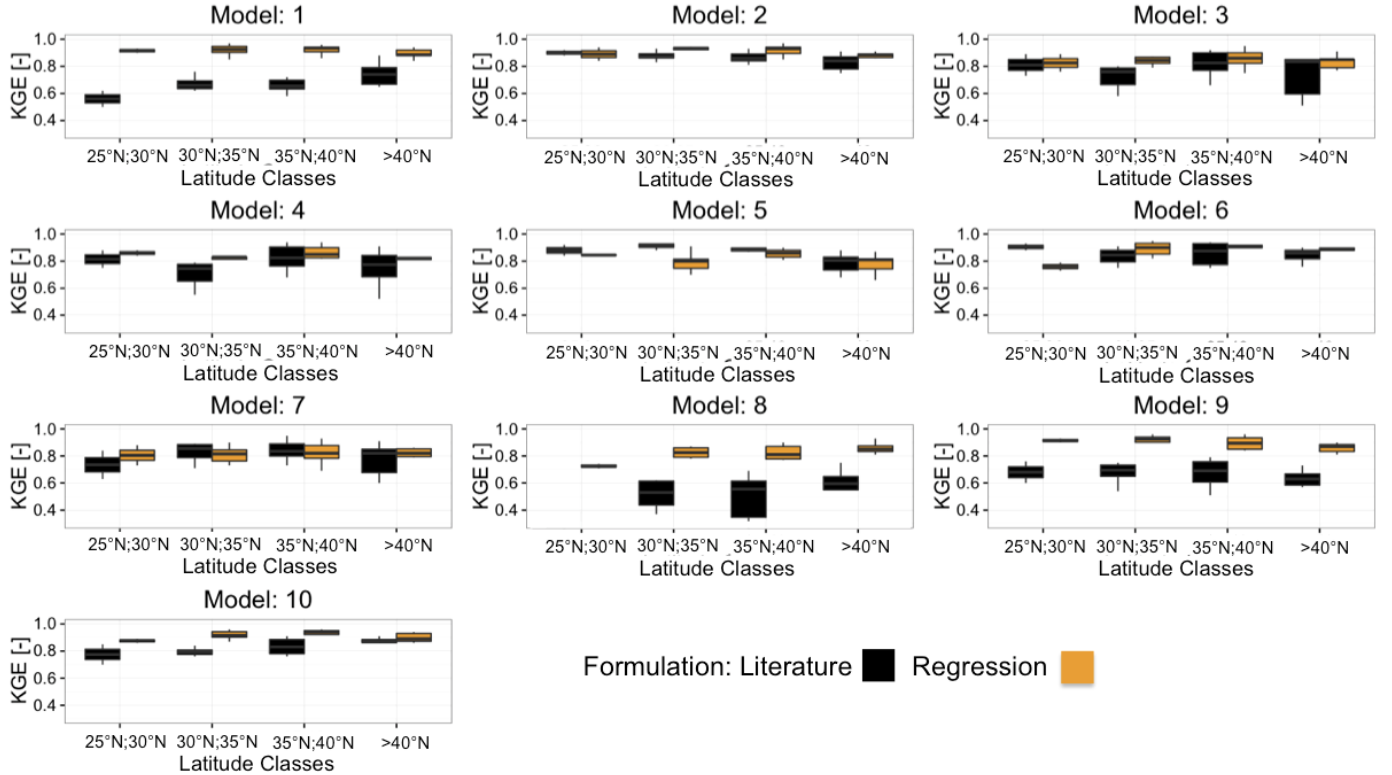


**Figure 8:** Comparison between model performances obtained with regression and classic parameters: the KGE values shown are those above 0.3 and results are grouped by latitude classes.

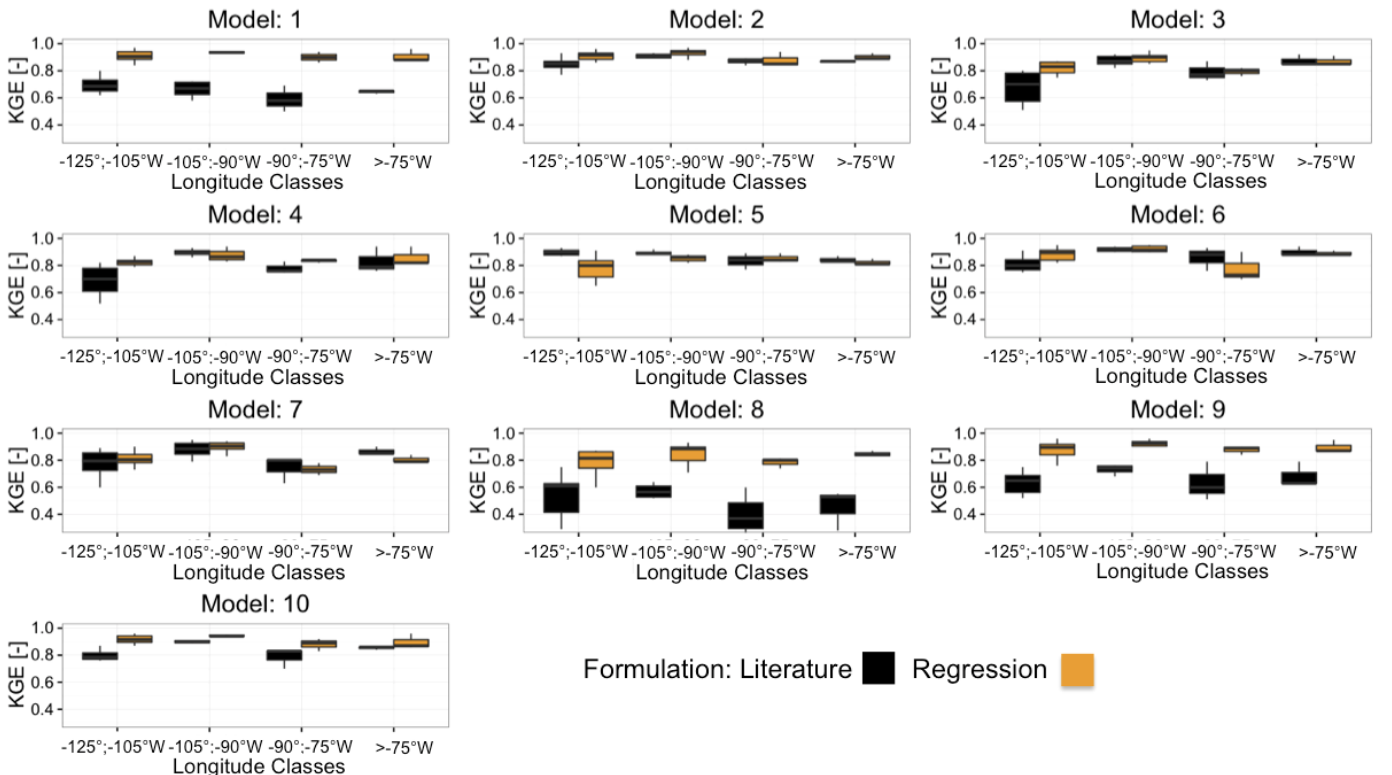


**Figure 9:** Comparison between model performances obtained with regression and classic parameters: the KGE values shown are those above 0.3 and results are grouped by longitude classes.

276 **4.5 Verification of the  $L_{\uparrow}$  model**

277 Figure 10 presents the results of the  $L_{\uparrow}$  simulations obtained using the three different temperatures available at  
278 experimental sites: soil surface temperature (skin temperature), air temperature, and soil temperature (mea-  
279 sured at 4 cm below the surface). The figure shows the performances of the  $L_{\uparrow}$  model for the three different  
280 temperatures used in terms of KGE, grouping all the stations for the whole simulation period according to  
281 season. This highlights the different behaviors of the model for periods where the differences in the three tem-  
282 peratures are larger (winter) or negligible (summer). The values of soil emissivity are assigned according the  
283 soil surface type, according to Table 4 (Brutsaert, 2005). Although many studies investigated the influence of  
284 snow covered area on longwave energy balance (e.g. Plüss and Ohmura (1997); Sicart et al. (2006)), the SMs  
285 do not explicitly take into account of it. As presented in König-Langlo and Augstein (1994), the effect of snow  
286 could be implicitly taken into account by tuning the emissivity parameter.

287 The best fit between measured and simulated  $L_{\uparrow}$  is obtained with the surface soil temperature, with an all-  
288 season average KGE of 0.80. Unfortunately, the soil surface temperature is not an easily available measurement.  
289 In fact, it is available only for 8 sites of the 24 in the study area. Very good results are also obtained using the  
290 air temperature, where the all-season average KGE is around 0.76. The results using air temperature present  
291 much more variance compared to those obtained with the soil surface temperature. However, air temperature  
292 (at 2 m height) is readily available measure, in fact it is available for all 24 sites.

293 The use soil temperature at 4 cm depth provides the least accurate results for our simulations, with an  
294 all-season average KGE of 0.46. In particular, the use of soil temperature at 4 cm depth during the winter is  
295 not able to capture the dynamics of  $L_{\uparrow}$ . It does, however, show a better fit during the other seasons. This could  
296 be because during the winter there is a substantial difference between the soil and skin temperatures, as also  
297 suggested in Park et al. (2008).

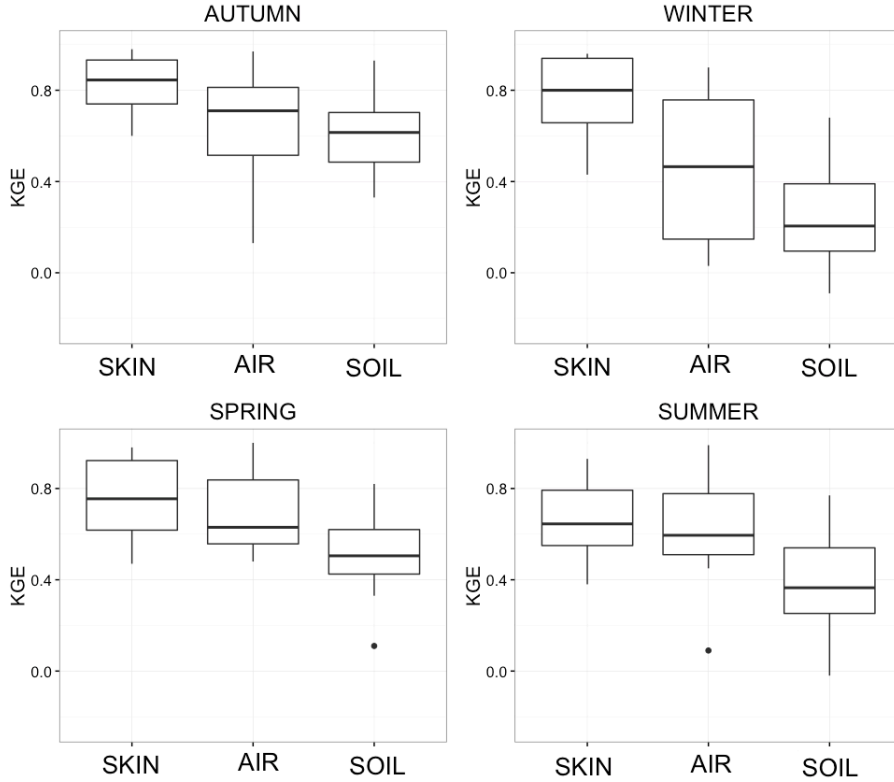


**Figure 10:** Boxplots of the KGE values obtained by comparing modeled upwelling longwave radiation, computed with different temperatures (soil surface temperature (SKIN), air temperature (AIR), and soil temperature (SOIL)), against measured data. Results are grouped by seasons.

## 298 5 Conclusions

299 This paper presents the LWRB package, a new modeling component integrated into the JGrass-NewAge system  
300 to model upwelling and downwelling longwave radiation. It includes ten parameterizations for the computation  
301 of  $L_{\downarrow}$  longwave radiation and one for  $L_{\uparrow}$ . The package uses all the features offered by the JGrass-NewAge  
302 system, such as algorithms to estimate model parameters and tools for managing and visualizing data in GIS.

303 The LWRB is tested against measured  $L_{\downarrow}$  and  $L_{\uparrow}$  data from 24 AmeriFlux test-sites located all over contiguous  
304 USA. The application for  $L_{\downarrow}$  longwave radiation involves model parameter calibration, model performance  
305 assessment, and parameters sensitivity analysis. Furthermore, we provide a regression model that estimates  
306 optimal parameter sets on the basis of local climatic variables, such as mean annual air temperature, rela-  
307 tive humidity, and precipitation. The application for  $L_{\uparrow}$  longwave radiation includes the evaluation of model  
308 performance using three different temperatures.

309 The main achievements of this work include: i) a broad assessment of the classic  $L_{\downarrow}$  longwave radiation  
310 parameterizations, which clearly shows that the Idso (1981) and Brunt (1932) models are the more robust and  
311 reliable for all the test sites, confirming previous results (Carmona et al., 2014); ii) a site specific assessment of  
312 the  $L_{\downarrow}$  longwave radiation model parameters for 24 AmeriFlux sites that improved the performances of all the  
313 models; iii) the set up of a regression model that provides an estimate of optimal parameter sets on the basis  
314 of climatic data; iv) an assessment of  $L_{\uparrow}$  model performances for different temperatures (skin temperature, air  
315 temperature, and soil temperature at 4 cm below surface), which shows that the skin and the air temperature

316 are better proxy for the  $L_{\uparrow}$  longwave radiation. Regarding longwave downwelling radiation the Brunt (1932)  
317 model is able to provide on average the best performances with the regression model parameters independently  
318 of the latitude and longitude classes. For the Idso (1981) model the formulation with regression parameter  
319 provided lower performances with respect to the literature formulation for latitude between 25°N and 30°N.

320 The integration of the package into JGrass-NewAge will allow users to build complex modeling solutions  
321 for various hydrological scopes. In fact, future work will include the link of the LWRB package to the existing  
322 components of JGrass-NewAge to investigate  $L_{\downarrow}$  and  $L_{\uparrow}$  effects on evapotranspiration, snow melting, and glacier  
323 evolution. Finally, the methodology proposed in this paper provides the basis for further developments such as  
324 the possibility to: i) investigate the effect of different all-sky emissivity formulation and quantify the influence of  
325 the clearness index threshold ii) verify the usefulness of the regression models for climates outside the contiguous  
326 USA; iii) analyze in a systematic way the uncertainty due to the quality of meteorological input data on the  
327 longwave radiation balance in scarce instrumented areas.

## 328 ACKNOWLEDGEMENTS

329 The authors are grateful to the AmeriFlux research community for providing the high-quality public data sets.  
330 In particular, we want to thank the principal investigators of each site: Shirley Kurc Papuga (AZ), Tilden  
331 P. Meyers (AZ), Russ Scott (AZ), Tom Kolb (AZ), Sonia Wharton (CA), Dennis D. Baldocchi (CA), Jordan  
332 G. Barr (FL), Vic C. Engel (FL), Jose D. Fuentes (FL), Joseph C. Zieman (FL), David Y. Hollinger (ME), Joe  
333 McFadden (MN), John M. Baker (MN), Timothy J. Griffis (MN), Lianhong Gu (MO), Kenneth L. Clark (NJ),  
334 Dave Billesbach (OK), James A. Bradford (OK), Margaret S. Torn (OK), James L. Heilman (TX), Ken Bible  
335 (WA), Sonia Wharton (WA). The authors thank the CLIMAWARE Project, of the University of Trento (Italy),  
336 and the GLOBAQUA Project, which have supported their research.

## 337 Replicable Research

338 The LWRB package has been implemented according to the object oriented paradigm, making them flexible,  
339 expendable for future improvements and maintenance. Thanks to Gradle Buid tool, an open source build  
340 automation system and Travis CI, a continuous integration service used to build and test software projects, the  
341 principle of the replicability of the research is fully satisfied. Researchers interested in replicating or extending  
342 our results are invited to download our codes at:

343 <https://github.com/geoframecomponents>.

344 Instructions for using the code can be found at:

345 <http://geoframe.blogspot.co.uk/2016/04/lwrb-component-latest-documentation.html>.

346 Regression of parameters were performed in R and are available at

347 [https://github.com/GEOframeOMSPProjects/OMS\\_Project\\_LWRB/blob/master/docs/Regression.R](https://github.com/GEOframeOMSPProjects/OMS_Project_LWRB/blob/master/docs/Regression.R)

## 348 References

349 Alados-Arboledas, L., Vida, J., and Olmo, F.: The estimation of thermal atmospheric radiation under cloudy  
350 conditions, *International journal of climatology*, 15, 107–116, 1995.

351 Ångström, A. K.: A study of the radiation of the atmosphere: based upon observations of the nocturnal  
352 radiation during expeditions to Algeria and to California, vol. 65, Smithsonian Institution, 1915.

353 Augustine, J. A., DeLuisi, J. J., and Long, C. N.: SURFRAD-A national surface radiation budget network for  
354 atmospheric research, *Bulletin of the American Meteorological Society*, 81, 2341–2357, 2000.

355 Augustine, J. A., Hodges, G. B., Cornwall, C. R., Michalsky, J. J., and Medina, C. I.: An update on SURFRAD-  
356 The GCOS Surface Radiation budget network for the continental United States, *Journal of Atmospheric and*  
357 *Oceanic Technology*, 22, 1460–1472, 2005.

358 Baldocchi, D., Falge, E., Gu, L., Olson, R., Hollinger, D., Running, S., Anthoni, P., Bernhofer, C., Davis, K.,  
359 Evans, R., et al.: FLUXNET: A new tool to study the temporal and spatial variability of ecosystem-scale  
360 carbon dioxide, water vapor, and energy flux densities, *Bulletin of the American Meteorological Society*, 82,  
361 2415–2434, 2001.

362 Barr, J. G., Engel, V., Smith, T. J., and Fuentes, J. D.: Hurricane disturbance and recovery of energy balance,  
363 CO<sub>2</sub> fluxes and canopy structure in a mangrove forest of the Florida Everglades, *Agricultural and Forest*  
364 *Meteorology*, 153, 54–66, 2012.

365 Bolz, H.: Die Abhängigkeit der infraroten Gegenstrahlung von der Bewölkung, *Z Meteorol*, 3, 201–203, 1949.

366 Brunt, D.: Notes on radiation in the atmosphere. I, *Quarterly Journal of the Royal Meteorological Society*, 58,  
367 389–420, 1932.

368 Brutsaert, W.: On a derivable formula for long-wave radiation from clear skies, *Water Resources Research*, 11,  
369 742–744, 1975.

370 Brutsaert, W.: *Hydrology: an introduction*, vol. 61, Wiley Online Library, 2005.

371 Campbell, G. S.: *Soil physics with BASIC: transport models for soil-plant systems*, vol. 14, Elsevier, 1985.

372 Carmona, F., Rivas, R., and Caselles, V.: Estimation of daytime downward longwave radiation under clear and  
373 cloudy skies conditions over a sub-humid region, *Theoretical and applied climatology*, 115, 281–295, 2014.

374 Chambers, J. M., Hastie, T., et al.: *Linear models*, 1992.

375 Corripi, J. G.: Modelling the energy balance of high altitude glacierised basins in the Central Andes, Ph.D.  
376 thesis, University of Edinburgh, 2002.

377 Crawford, T. M. and Duchon, C. E.: An improved parameterization for estimating effective atmospheric emis-  
378 sivity for use in calculating daytime downwelling longwave radiation, *Journal of Applied Meteorology*, 38,  
379 474–480, 1999.

380 David, O., Ascough, J., Lloyd, W., Green, T., Rojas, K., Leavesley, G., and Ahuja, L.: A software engineering  
381 perspective on environmental modeling framework design: The Object Modeling System, *Environmental  
382 Modelling & Software*, 39, 201–213, 2013.

383 Dilley, A. and O'brien, D.: Estimating downward clear sky long-wave irradiance at the surface from screen  
384 temperature and precipitable water, *Quarterly Journal of the Royal Meteorological Society*, 124, 1391–1401,  
385 1998.

386 Duan, Q., Gupta, V. K., and Sorooshian, S.: Shuffled complex evolution approach for effective and efficient  
387 global minimization, *Journal of optimization theory and applications*, 76, 501–521, 1993.

388 Efron, B. and Efron, B.: The jackknife, the bootstrap and other resampling plans, vol. 38, SIAM, 1982.

389 Flerchinger, G.: The Simultaneous Heat and Water (SHAW) Model: Technical Documentation, Northwest  
390 Watershed Research Center, USDA Agricultural Research Service, Boise, Tech. rep., Idaho, Technical Report  
391 NWRC 2000-09, 37 pp, 2000.

392 Flerchinger, G., Xaio, W., Marks, D., Sauer, T., and Yu, Q.: Comparison of algorithms for incoming atmospheric  
393 long-wave radiation, *Water resources research*, 45, 2009.

394 Formetta, G., Rigon, R., Chávez, J., and David, O.: Modeling shortwave solar radiation using the JGrass-  
395 NewAge system, *Geoscientific Model Development*, 6, 915–928, 2013.

396 Formetta, G., Antonello, A., Franceschi, S., David, O., and Rigon, R.: Hydrological modelling with components:  
397 A GIS-based open-source framework, *Environmental Modelling & Software*, 55, 190–200, 2014a.

398 Formetta, G., David, O., and Rigon, R.: Testing site-specific parameterizations of longwave radiation integrated  
399 in a GIS-based hydrological model, International Environmental Modelling and Software Society (iEMSS) 7th  
400 Intl. Congress on Env. Modelling and Software, San Diego, CA, USA, Daniel P. Ames, Nigel W.T. Quinn  
401 and Andrea E. Rizzoli (Eds.), 2014b.

402 Gupta, H. V., Kling, H., Yilmaz, K. K., and Martinez, G. F.: Decomposition of the mean squared error and  
403 NSE performance criteria: Implications for improving hydrological modelling, *Journal of Hydrology*, 377,  
404 80–91, 2009.

405 Hatfield, J., Reginato, R. J., and Idso, S.: Comparison of long-wave radiation calculation methods over the  
406 United States, *Water Resources Research*, 19, 285–288, 1983.

407 Hay, L. E., Leavesley, G. H., Clark, M. P., Markstrom, S. L., Viger, R. J., and Umemoto, M.: Step wise,  
408 multiple objective calibration of a hydrologic model for a snowmelt dominated basin1, 2006.

409 Idso, S. B.: A set of equations for full spectrum and 8-to 14- $\mu$ m and 10.5-to 12.5- $\mu$ m thermal radiation from  
410 cloudless skies, *Water resources research*, 17, 295–304, 1981.

411 Idso, S. B. and Jackson, R. D.: Thermal radiation from the atmosphere, *Journal of Geophysical Research*, 74,  
412 5397–5403, 1969.

413 Iziomon, M. G., Mayer, H., and Matzarakis, A.: Downward atmospheric longwave irradiance under clear and  
414 cloudy skies: Measurement and parameterization, *Journal of Atmospheric and Solar-Terrestrial Physics*, 65,  
415 1107–1116, 2003a.

416 Iziomon, M. G., Mayer, H., and Matzarakis, A.: Downward atmospheric longwave irradiance under clear and  
417 cloudy skies: Measurement and parameterization, *Journal of Atmospheric and Solar-Terrestrial Physics*, 65,  
418 1107–1116, 2003b.

419 Jacobs, J.: Radiation climate of Broughton Island, *Energy budget studies in relation to fast-ice breakup pro-*  
420 *cesses in Davis Strait*, 26, 105–120, 1978.

421 Juszak, I. and Pellicciotti, F.: A comparison of parameterizations of incoming longwave radiation over melting  
422 glaciers: model robustness and seasonal variability, *Journal of Geophysical Research: Atmospheres*, 118,  
423 3066–3084, 2013.

424 Keding, I.: *Klimatologische Untersuchung ueber die atmosphaerische Gegenstrahlung und Vergleich vom Berech-*  
425 *nungsverfahren anhand langjaehriger Messungen im Oberrheintal*, Offenbach am Main: Selbstverlag des  
426 Deutschen Wetterdienstes, 1989.

427 Kelliher, F., Ross, D., Law, B., Baldocchi, D., and Rodda, N.: Limitations to carbon mineralization in litter  
428 and mineral soil of young and old ponderosa pine forests, *Forest Ecology and Management*, 191, 201–213,  
429 2004.

430 Key, J. R. and Schweiger, A. J.: Tools for atmospheric radiative transfer: Streamer and FluxNet, *Computers*  
431 & *Geosciences*, 24, 443–451, 1998.

432 Kneizys, F. X., Shettle, E., Abreu, L., Chetwynd, J., and Anderson, G.: Users guide to LOWTRAN 7, Tech.  
433 rep., DTIC Document, 1988.

434 König-Langlo, G. and Augstein, E.: Parameterization of the downward long-wave radiation at the Earth's  
435 surface in polar regions, *Meteorologische zeitschrift*, NF 3, Jg. 1994, H. 6, pp. 343–347, 1994.

436 Konzelmann, T., van de Wal, R. S., Greuell, W., Bintanja, R., Henneken, E. A., and Abe-Ouchi, A.: Parameter-  
437 ization of global and longwave incoming radiation for the Greenland Ice Sheet, *Global and Planetary change*,  
438 9, 143–164, 1994.

439 Leigh Jr, E. G.: *Tropical Forest Ecology: A View from Barro Colorado Island: A View from Barro Colorado*  
440 Island, Oxford University Press, 1999.

441 MacDonell, S., Nicholson, L., and Kinnard, C.: Parameterisation of incoming longwave radiation over glacier  
442 surfaces in the semiarid Andes of Chile, *Theoretical and applied climatology*, 111, 513–528, 2013.

443 Maykut, G. A. and Church, P. E.: Radiation climate of Barrow Alaska, 1962-66, *Journal of Applied Meteorology*,  
444 12, 620–628, 1973.

445 Monteith, J. L. and Unsworth, M.: *Principles of Environmental Physics*, Butterworth-Heinemann, 1990.

446 Niemelä, S., Räisänen, P., and Savijärvi, H.: Comparison of surface radiative flux parameterizations: Part I:  
447 Longwave radiation, *Atmospheric Research*, 58, 1–18, 2001.

448 Park, G.-H., Gao, X., and Sorooshian, S.: Estimation of surface longwave radiation components from ground-  
449 based historical net radiation and weather data, *Journal of Geophysical Research: Atmospheres* (1984–2012),  
450 113, 2008.

451 Plüss, C. and Ohmura, A.: Longwave radiation on snow-covered mountainous surfaces, *Journal of Applied*  
452 *Meteorology*, 36, 818–824, 1997.

453 Prata, A.: A new long-wave formula for estimating downward clear-sky radiation at the surface, *Quarterly*  
454 *Journal of the Royal Meteorological Society*, 122, 1127–1151, 1996.

455 Rotenberg, E., Mamane, Y., and Joseph, J.: Long wave radiation regime in vegetation-parameterisations for  
456 climate research, *Environmental modelling & software*, 13, 361–371, 1998.

457 Schmucki, E., Marty, C., Fierz, C., and Lehning, M.: Evaluation of modelled snow depth and snow water equiva-  
458 lent at three contrasting sites in Switzerland using SNOWPACK simulations driven by different meteorological  
459 data input, *Cold Regions Science and Technology*, 99, 27–37, 2014.

460 Sicart, J.-E., Pomeroy, J., Essery, R., and Bewley, D.: Incoming longwave radiation to melting snow: observa-  
461 tions, sensitivity and estimation in northern environments, *Hydrological processes*, 20, 3697–3708, 2006.

462 Sugita, M. and Brutsaert, W.: Cloud effect in the estimation of instantaneous downward longwave radiation,  
463 *Water Resources Research*, 29, 599–605, 1993a.

464 Sugita, M. and Brutsaert, W.: Comparison of land surface temperatures derived from satellite observations  
465 with ground truth during FIFE, *International Journal of Remote Sensing*, 14, 1659–1676, 1993b.

466 Swinbank, W. C.: Long-wave radiation from clear skies, *Quarterly Journal of the Royal Meteorological Society*,  
467 89, 339–348, 1963.

468 Unsworth, M. H. and Monteith, J.: Long-wave radiation at the ground I. Angular distribution of incoming  
469 radiation, *Quarterly Journal of the Royal Meteorological Society*, 101, 13–24, 1975.

470 Wilkinson, G. and Rogers, C.: Symbolic description of factorial models for analysis of variance, *Applied Statis-  
471 tics*, pp. 392–399, 1973.

472 Xiao, J., Zhuang, Q., Law, B. E., Chen, J., Baldocchi, D. D., Cook, D. R., Oren, R., Richardson, A. D.,  
473 Wharton, S., Ma, S., et al.: A continuous measure of gross primary production for the conterminous United  
474 States derived from MODIS and AmeriFlux data, *Remote sensing of environment*, 114, 576–591, 2010.